



HAL
open science

PARP2 deficiency affects invariant-NKT,-cell maturation and protects mice from ,Concanavalin A-induced liver injury.

Aveline Filliol, Claire Piquet-Pellorce, Sarah Dion, Valentine Genet, Catherine Lucas-Clerc, Françoise Dantzer, Michel Samson

► To cite this version:

Aveline Filliol, Claire Piquet-Pellorce, Sarah Dion, Valentine Genet, Catherine Lucas-Clerc, et al.. PARP2 deficiency affects invariant-NKT,-cell maturation and protects mice from ,Concanavalin A-induced liver injury.. *AJP - Gastrointestinal and Liver Physiology*, 2017, 313 (5), pp.G399-G409. 10.1152/ajpgi.00436.2016 . hal-01630440

HAL Id: hal-01630440

<https://univ-rennes.hal.science/hal-01630440v1>

Submitted on 7 Nov 2017

HAL is a multi-disciplinary open access archive for the deposit and dissemination of scientific research documents, whether they are published or not. The documents may come from teaching and research institutions in France or abroad, or from public or private research centers.

L'archive ouverte pluridisciplinaire **HAL**, est destinée au dépôt et à la diffusion de documents scientifiques de niveau recherche, publiés ou non, émanant des établissements d'enseignement et de recherche français ou étrangers, des laboratoires publics ou privés.

1 **PARP2 deficiency affects invariant-NKT-cell maturation and protects mice from**
2 **Concanavalin A-induced liver injury.**

3

4 Aveline Filliol^{1,2,3}, Claire Piquet-Pellorce^{1,2,3}, Sarah Dion^{1,2,3}, Valentine Genet^{1,2,3},
5 Catherine Lucas-Clerc^{2,4}, Françoise Dantzer⁵, and Michel Samson^{1,2,3}.

6

7 ¹Institut National de la Santé et de la Recherche Médicale (Inserm), U.1085, Institut de Recherche
8 Santé Environnement et Travail (IRSET), F-35043 Rennes, France.

9 ²Université de Rennes 1, F-35043 Rennes, France.

10 ³Structure Fédérative BioSit UMS 3480 CNRS-US18 Inserm, F-35043 Rennes, France.

11 ⁴Service de Biochimie CHU Rennes, Université de Rennes 1; F-35043 Rennes, France.

12 ⁵Université de Strasbourg, Biotechnologie et Signalisation Cellulaire, UMR7242 CNRS, Laboratoire
13 d'Excellence Medalis, ESBS, 300, Boulevard Sébastien-Brant, CS 10413, 67412 Illkirch, France.

14

15 **Correspondence:** Michel Samson, INSERM-U1085, IRSET, Université de Rennes 1,
16 2, Avenue du Professeur Léon Bernard, 35043 RENNES Cedex, France. Phone
17 (+33) 22 323 5927 ; Fax (+33) 22 323 4794.

18

19 **Number of figures:** 6

20 **Number of tables:** 1

21

22 **Financial support:** This work was supported by INSERM, the Ministère de

23 l'Education Nationale, de l'Enseignement Supérieur et de la Recherche, the
24 Université de Rennes 1, the Région Bretagne, the "Ligue Contre le Cancer, Comités
25 du Grand Ouest".

26

27 **Conflict of interest:** The authors declare no financial or commercial conflict of
28 interest.

29

30 **Keywords:** Hepatitis, Parp, Liver, NKT cells, Autoimmune hepatitis

31

32 **List of abbreviations:**

33 α -GalCer: α -Galactosylceramide, ConA: Concanavalin A, DAMPs: Damage
34 Associated Molecular Patterns, DN: double negative, DR: death receptors, NKT:
35 Natural Killer-T, NK: Natural Killer, PARP: poly(ADP) ribose polymerase.

36

37 a. Conflict of interest.

38

39 Aveline Filliol declares no financial or commercial conflict of interest.

40 Claire Piquet-Pellorce declares no financial or commercial conflict of interest.

41 Sarah Dion declares no financial or commercial conflict of interest.

42 Valentine Genet declares no financial or commercial conflict of interest.

43 Catherine Lucas-Clerc declares no financial or commercial conflict of interest.

44 Françoise Dantzer declares no financial or commercial conflict of interest.

45 Michel Samson declares no financial or commercial conflict of interest.

46

47 b. Authors' contributions

48

- 49 Aveline Filliol : acquisition of data; analysis and interpretation of data, statistical analysis,
50 drafting of the manuscript
- 51 Claire Piquet-Pellorce : acquisition of data, analysis and interpretation of data
- 52 Sarah Dion : acquisition of data, analysis and interpretation of data
- 53 Valentine Genet : acquisition of data and analysis
- 54 Catherine Lucas-Clerc : obtained technical or material support
- 55 Françoise Dantzer: drafting of the manuscript, critical revision of the manuscript for important
56 intellectual content
- 57 Michel Samson: acquisition of data, analysis and interpretation of data, statistical analysis,
58 drafting of the manuscript, study concept and design, study supervision
- 59

60 **Abstract (202 words)**

61 Excessive or persistent inflammation and hepatocyte death are the key triggers of
62 liver diseases. The poly(ADP-ribose) polymerase (PARP) proteins induce cell death
63 and inflammation. Chemical inhibition of PARP activity protects against liver injury
64 during Concanavalin A (ConA)-induced hepatitis. In this mice model, ConA activates
65 immune cells which promote inflammation and induce hepatocyte death, mediated by
66 the activated invariant NKT-(iNKT) lymphocyte population. We analyzed immune cell
67 populations in the liver and several lymphoid organs such as spleen, thymus, and
68 bone marrow in *Parp2* deficient mice to better define the role of PARP proteins in
69 liver immunity and inflammation at steady state and during ConA-induced hepatitis.
70 We show that *i*) the genetic inactivation of *Parp2*, but not *Parp1*, protected mice from
71 ConA hepatitis without deregulating cytokine expression and leucocyte recruitment;
72 *ii*) cellularity was lower in the thymus, but not in spleen, liver, or bone marrow of
73 *Parp2*^{-/-} mice; *iii*) spleen and liver iNKT lymphocytes, as well as thymic T and NKT
74 lymphocytes were reduced in *Parp2* knockout mice. In conclusion, our results
75 suggest that the defect of T-lymphocyte maturation in *Parp2* knockout mice leads to a
76 systemic reduction of iNKT cells, reducing hepatocyte death during ConA-mediated
77 liver damage, thus protecting the mice from hepatitis.

78

79 INTRODUCTION

80 Hepatitis can be caused by various insults such as alcohol, a high fat diet, food-
81 derived toxins, or infections, and is characterized by hepatocyte death and
82 inflammation (5). Acute hepatitis is associated with massive hepatolysis which can
83 lead to liver failure, whereas in chronic hepatitis, unresolved hepatolysis triggers the
84 release of Damage Associated Molecular Patterns (DAMPs) which promote
85 inflammation. This process induces an inflammation and cell death amplification loop
86 that contributes to the progression of liver diseases (5, 18). Blocking the pro-
87 inflammatory hepatocyte death response could be beneficial to in treating liver
88 diseases.

89 During viral or auto-immune hepatitis, innate and adaptive lymphocytes kill
90 hepatocytes which present proteins recognized as non-self-antigens, by the
91 activation of death receptors (DR). In mice, Concanavalin A (ConA)-induced liver
92 injury mimics immune cell-mediated hepatitis in humans (27) and is dependent on
93 innate Natural Killer T (NKT) lymphocytes. NKT cells are involved in numerous
94 immune responses and are particularly abundant in the liver and spleen of mice.
95 They have the ability to recognize lipids presented by CD1d which allows there
96 distinction into two categories of NKT cells. Type I or invariant-NKT (iNKT) cells
97 express an invariant T-cell receptor α -chain (TCR α ; V α 14-J α 18) and are able to
98 recognize the α -Galactosylceramide (α -GalCer) presented by CD1d. Type II NKT
99 cells express more diverse TCR V α chains that cannot recognize α -GalCer and are
100 characterized as CD4/CD8 double negative (DN). The iNKT are the major NKT
101 subset in the liver and CD1d^{-/-} (NKT deficient) mice as well as V α 14^{-/-} (iNKT deficient)
102 mice are protected from ConA-induced hepatitis (15, 26-28). ConA activates liver
103 immune cells which promote hepatocyte death in two ways. First, activated immune

104 cells release large amounts of cytokines, such as TNF- α (17, 21), IFN- γ (12, 25) and
105 IL-4 (13) which play key roles in the hepatocyte death process (17, 27, 29). Second,
106 activated NKT cells, potent producers of IFN- γ , kill hepatocytes by activation of the
107 TNF-superfamily DR (3, 23, 26, 33) and the perforin/granzyme B system (31). Our
108 group has extensively investigated the mechanisms of hepatocyte death during
109 hepatitis. We and others have demonstrated a key role for PARP proteins in the liver.
110 We have shown that inhibition of poly(ADP) ribose polymerase (PARP) 1 and 2
111 activity with the PJ-34-inhibitor protects mice from ConA-mediated hepatolysis (2,
112 14). Mukhopadhyay *et al.* have shown that genetic or chemical inhibition of PARP1
113 also prevents liver inflammation and fibrosis induced by the hepatotoxic carbon
114 tetrachloride (CCl₄) or bile duct ligation (22). PARP1 and PARP2 are activated by
115 DNA strand breaks and use NAD⁺ as a substrate to synthesize chains of
116 poly(ADPribose) onto various acceptor proteins, thereby inducing chromatin
117 remodeling and the recruitment of DNA repair complexes (8). In the last decades,
118 PARP1 and PARP2 have also been found to play an important role in inflammation
119 (4) and cell death (30). In this study, we aimed to better define the roles of PARP1
120 and PARP2 proteins in ConA-induced hepatitis using the *Parp1* and *Parp2* knockout
121 mouse models.

122

123 **METHODS**

124 **Animals and treatment protocols**

125 C57BL/6 *Parp1* and *Parp2* genetically modified mice (*Parp1*^{-/-} and *Parp2*^{-/-},
126 respectively) were provided by Dr. F. Dantzer and generated as described previously
127 (7, 32). Heterozygous mice were crossed to obtain knockout and littermate WT mice.
128 Adult male and female mice, of 10 to 12 weeks of age, were used for each

129 experiment with the ConA model. ConA (C2010 Sigma-Aldrich, St. Louis, MO) was
130 prepared at 3 mg/mL in PBS supplemented with 0.31 mM MnCl₂ and 0.75 mM CaCl₂
131 and administered by intravenous (i.v.) injection at a dose of 10 or 12 mg/kg body
132 weight. For histopathological and biochemical studies, mice treated with ConA were
133 compared to mice which received PBS supplemented with 0.31 mM MnCl₂ and 0.75
134 mM CaCl₂. For all phenotypic immune cell analyses, adult (10 to 12 weeks old) or
135 early adult (five- week-old) mice were either not treated, to analyze the population at
136 steady state, or treated with ConA. Animals were housed in individual cages and
137 bred in specific pathogen-free conditions in the local animal house facilities. All
138 treatment protocols were in accordance with the French laws and the institution's
139 guidelines for animal welfare (agreement of M. Samson # R-2012-CPP-01).

140

141 **Histopathological and biochemical studies**

142 Mouse liver biopsies were fixed in 4% paraformaldehyde and embedded in paraffin
143 for IHC and hematoxylin and eosin (H&E) staining. For histopathology, H&E staining
144 of liver tissues was carried out to investigate liver injury. Serum ALT and AST
145 transaminases were measured according to the IFCC primary reference procedures
146 using an Olympus AU2700 Autoanalyser[®] (Olympus Optical, Tokyo, Japan).

147

148 **RNA analysis**

149 Total RNA was extracted from mouse livers using TRIzol reagent (Invitrogen). First-
150 strand cDNA was synthesized using the SuperScript[™] II Reverse Transcriptase
151 (Invitrogen). Real-time quantitative PCR was performed using the fluorescent dye

152 SYBR Green with the double-strand specific SYBR[®] Green system (Applied
153 Biosystems) and the ABI 7000 Prism sequence detector (Applied Biosystems) or the
154 CFX384 Touch™ Real-Time PCR Detection System (Bio-Rad). cDNA was used as
155 template for amplification using specific primer pairs (Table 1). Each measurement
156 was performed in triplicate. The relative gene expression was normalized against
157 18S rRNA gene expression. The control mice in each treatment group served as a
158 reference for messenger RNA (mRNA) expression (the control mRNA level was
159 arbitrarily set to 1).

160

161 **Immune cell analysis by flow cytometry**

162 Immune cells were prepared from spleen, thymus, or liver crushed on a 70 µm filter.
163 Liver immune cells were isolated after sedimentation and cell fractionation on a 35%
164 Percoll layer. For each organ, red blood cells were lysed using ammonium-chloride-
165 potassium (ACK) buffer. Bone marrow immune cells were isolated by flushing two
166 femurs with RPMI medium (Gibco). The number of immune cells was determined by
167 counting in a Malassez counting chamber.

168 Cell suspensions were labeled for 30 min with LIVE/DEAD fixable yellow stain (Life
169 technologies, L34959) to exclude dead cells from the analysis. Cells were also pre-
170 incubated with an anti-CD16/32 antibody (BD Pharmingen) to block non-specific
171 binding before incubation with the appropriate fluorochrome-conjugated antibodies
172 (BD Pharmingen, eBioscience): anti-CD3-FITC (clone 17A2), anti-TCRβ-V450 (clone
173 H57-597), anti-CD69-PE (clone H1.2F3), anti-CD19-APC or anti-CD19-PE (clone
174 1D3), anti-NK1.1-PerCP-Cy-5.5 (clone PK136), anti-CD4-PE-Cy7 (clone RM4-5),
175 anti-CD8-APC-Cy7 (clone 53-6.7), anti-GR1-eFluor450 (clone FB6-8C5), anti-

176 CD11b-PE-Cy7 (clone M1/70), anti-Sca1-PE (clone D7), anti-c-kit-PerCP-eFluor710
177 (clone 2B8), anti-Ter119-eFluor780 (clone Ter119), and empty CD1d tetramer or
178 CD1d tetramer loaded with α -galactosylceramide (GalCer)-PE (provided by Dr. M.
179 Leite de Moraes). The stained cells were analyzed on a FACSAria™ II flow
180 cytometer and data were analyzed using CXP software (Beckman Coulter). Doublets
181 and dead cells were excluded on the basis of forward/side scatter and LIVE/DEAD
182 labeling, respectively. The immuno-phenotyping used was as follows: B-lymphocytes:
183 CD19+/CD3- cells; T-lymphocytes: CD3+/TCRV β +/NK1.1-; NKT cells:
184 CD3+/TCRV β +/NK1.1+; NK cells: CD3-/NK1.1+; and granulocytes: GR1+CD11b+.
185 Lymphoid activation was studied by analyzing the expression of CD69. We calculated
186 the percentage of each immune cell population, by considering the sum of events of
187 all immune cell populations analyzed (sum of T, NK, NKT, B cells and myeloid cells)
188 as 100% of the total immune cells. The absolute number in each immune cell
189 population was calculated by multiplying the percentage of each population by the
190 total number of immune cells.

191

192 **Serum cytokine immunoassay by flow cytometry**

193 Murine TNF- α , IFN- γ and IL-6 cytokines were quantified by bead-based
194 immunoassays according to manufacturer protocol, using a filter plate and a vacuum
195 filtration system for washing steps (BioLegend's LEGENDPLEX, multi-analyte flow
196 assay kit). Samples were analyzed on a LSR Fortessa cytometer (BD Biosciences).

197

198 **Statistical analysis**

199 Data are expressed as the means +/- SEM for all mice treated similarly. Kruskal–
200 Wallis one-way analysis of variance (ANOVA) was performed, and mean differences
201 between experimental groups were assessed using the non-parametric Mann–
202 Whitney *U*-test using GraphPad Prism5 software.

203

204 **RESULTS**

205

206 **PARP2 but not PARP1 deficiency protects mice from ConA-induced hepatitis**

207 We investigated the role of PARP1 and PARP2 proteins in hepatitis using adult
208 knockout mice for PARP1 (*Parp1*^{-/-}) and PARP2 (*Parp2*^{-/-}) and comparing the results
209 to those obtained using wild-type mice (WT). We challenged mice with ConA to
210 induce hepatitis, or with PBS as a control, and evaluated liver damage using serum
211 transaminase (ALT and AST) levels and hematoxylin coloration. In ConA induced-
212 hepatitis, the peak of hepatolysis occurs 11 h after ConA treatment.(29) *Parp1*^{-/-} mice
213 displayed visibly, but non-significantly, lower ALT and AST transaminase levels than
214 WT mice at this time point. In contrast, *Parp2*^{-/-} mice were highly protected from
215 ConA-induced hepatitis as they had significantly lower (4-fold) levels of both AST and
216 ALT than WT mice (Fig. 1A). Accordingly, H&E coloration of liver slides from Con A-
217 treated WT and *Parp2*^{-/-} mice, revealed fewer areas of necrosis in *Parp2* deficient
218 mice than in WT mice (Fig. 1B). Moreover, the absence of PARP2 appeared to
219 protect mice from hepatolysis and did not simply delay liver injury as serum
220 transaminase levels remained significantly lower in *Parp2*^{-/-} mice than in WT mice,
221 even 24 h after ConA administration (Fig. 1C). We next evaluated the level of
222 inflammation induced by ConA, by measuring the mRNA levels of TNF- α , IFN- γ , IL-
223 1 β , and IL-4, all known to play key roles during ConA-induced hepatitis. TNF- α , IFN-

224 γ , IL-1 β , and IL-4 transcript levels were higher in all genotypes after ConA treatment.
225 However, we observed no significant differences between the IFN- γ or IL-4 mRNA
226 levels in *Parp1*^{-/-}, *Parp2*^{-/-}, or WT mice, whereas TNF- α transcript levels were
227 significantly lower in *Parp2*^{-/-} mice than in the other two mouse strains. In contrast, IL-
228 1 β mRNA levels were higher in both *Parp2*^{-/-} and *Parp1*^{-/-} mice than in WT mice.
229 Next, we analyze serum cytokines from WT and *Parp2*^{-/-} mice. TNF- α , IFN- γ and IL-
230 6 were up-regulated in both genotypes after ConA challenge. However, TNF- α and
231 IFN- γ levels were similar between WT and *Parp2*^{-/-} mice, whereas IL-6 rate
232 decreased in *Parp2*^{-/-} mice (Fig. 1E).

233

234 ***Parp2*^{-/-} mice display a substantial reduction in the number of liver iNKT cells**

235 We performed all further experiments using only the *Parp2*^{-/-} mouse model, as
236 PARP2 protein deficiency protected mice from ConA-induced liver damage, whereas
237 that of PARP1 did not. ConA induces liver injury in an immune cell-dependent
238 manner. Thus we next measured the steady-state, basal levels of the different liver
239 immune cell subsets in *Parp2*^{-/-} mice of two different ages: early adult (five weeks)
240 and adult (10 to 12 weeks) by flow cytometry. Cell doublets and dead cells were
241 excluded and the phenotypic analysis of liver immune cells was determined using the
242 gating strategy presented in Figure 2A.

243 *Parp2*^{-/-} mice displayed a similar number of liver immune cells as WT mice at the two
244 different ages (Fig. 2B). The absolute number of total T lymphocytes and the ratio of
245 CD4:CD8 T-lymphocytes were also similar in the livers of both genotypes (Fig. 2C).
246 We next analyzed the NKT-lymphocyte population, defined as CD3, TCRV β , and
247 NK1.1 positive cells. We used the CD1d tetramer loaded with α GalCer to analyze the
248 invariant-NKT (iNKT) subset (CD3⁺ TCRV β ⁺ NK1.1⁺ α GalCer⁺) and the anti-CD4

249 antibody to study NKT DN cells (CD3⁺ TCRV β ⁺ NK1.1⁺ α GalCer⁻ CD4⁻). *Parp2*^{-/-}
250 mice displayed a reduction in the percentage of total liver NKT cells of two fold in
251 five-week-old mice and of 1.5 fold in 10-12-week-old mice (Fig. 2D). However,
252 PARP2 deficiency did not impair the increase in the percentage of liver NKT cells as
253 the mice aged (Fig 2D). We also observed that only the percentage of iNKT cells, but
254 not NKT DN cells, was significantly lower in the *Parp2*^{-/-} mice at both ages (Fig. 2E).
255 The absolute number of liver immune cells was similar between both genotypes,
256 whereas the number of iNKT cells was lower in *Parp2*^{-/-} mice. We thus aimed to
257 determine which immune cell subsets compensated this reduction. The percentage of
258 NK-cells (NK1.1⁺ CD3⁻) and B-lymphocytes (CD19⁺ CD11b⁻) were higher in five-
259 week-old *Parp2*^{-/-} mice, but only the percentage of NK-cells was higher in adult *Parp2*
260 ^{-/-} mice (Fig. 2F and 2G). The liver myeloid compartment, based on GR1 and CD11b
261 labelling, also appeared to be similar in *Parp2*^{-/-} and WT mice, regardless of age (Fig.
262 2H). In conclusion, PARP2 deficiency induced a significant reduction in the number of
263 iNKT cells in the liver which was not compensated by an increase of all immune cell
264 subsets, but by a gain of B and NK-lymphocytes.

265

266 **PARP2 deficiency does not affect the recruitment and activation of immune**
267 **cells during ConA-induced hepatitis.**

268 We next examined the impact of PARP2 deficiency on ConA-induced cell recruitment
269 and activation. ConA-induced inflammation and cell death induced a similarly high
270 level of leucocyte recruitment to the liver in mice of both genotypes as seen by the
271 large increase in the absolute number of liver immune cells 11 h after injection, which
272 then decreased with the resolution of the hepatitis 24 h after ConA treatment (Fig.
273 3A). We evaluated the NKT-cell subset and found a reduction in the number of NKT

274 cells in the livers of mice of both genotypes upon ConA treatment. However, this
275 reduction was 3.7 fold in WT mice, relative to untreated mice, but only 1.7 fold in
276 *Parp2*^{-/-} mice, (Fig. 3B). The absence of PARP2 protein did not seem to affect the
277 recruitment of other leucocyte populations, as T, B, and NK-lymphocytes, and
278 myeloid cells were similarly recruited for both genotypes 11 h after ConA
279 administration (Fig. 3C). Finally, we analyzed the early activation marker CD69 on
280 lymphocytes and observed that more than 90% of T-lymphocytes in both *Parp2*^{-/-} and
281 WT mice were activated after ConA treatment (Fig. 3D).

282

283 ***Parp2*^{-/-} mice have fewer spleen iNKT cells than WT mice**

284 We demonstrated that *Parp2*^{-/-} mice were protected from ConA-hepatitis and had
285 fewer hepatic NKT cells, without affecting ConA-induced inflammation. We next
286 analyzed the immune cell subsets in the various lymphoid compartments such as
287 spleen, bone marrow, and thymus. Gating strategies used for splenocyte analysis are
288 depicted in Supplementary Figures 1 and 2. PARP2 deficiency did not affect the
289 absolute number of splenocytes in mature mice but they were slightly, but not
290 significantly, higher in number in early adult mice (Fig. 4A). We then evaluated the
291 percentage cells in each immune cell subset in the spleen. The number of T-
292 lymphocytes (CD3⁺ NK1.1⁻ TCRVβ⁺) were lower only in early adult *Parp2*^{-/-} mice
293 (Fig. 4B) and was compensated by an increase in the number of B-lymphocytes
294 (CD19⁺ CD11b⁻) (Fig. 4C). Similar to our observations in the liver, the spleens of
295 five- and 10-12-week-old *Parp2*^{-/-} mice had significantly fewer NKT cells than those of
296 WT mice, and only the iNKT cells were affected (Fig. 4D). In contrast to the liver, the
297 number of spleen NK cells was only slightly, but not significantly, higher in *Parp2*^{-/-}
298 than in WT mice (Fig. 4E).

299

300 ***Parp2*^{-/-} mice have fewer thymus iNKT cells than WT mice.**

301 We next investigated the thymocyte population of five-week-old mice to understand
302 the cause of the reduction in NKT-cell number in the liver and spleen of *Parp2*^{-/-} mice.
303 The absolute number of thymocytes was lower in *Parp2*^{-/-} mice than in WT mice, and
304 was associated with a reduction in the absolute number of immature CD4/CD8
305 double positive (DP) and CD4 or CD8 simple positive (SP) thymocytes (Fig. 5A and
306 5B). The absolute number of iNKT cells (α GalCer⁺) was also lower in *Parp2*^{-/-} mice
307 (Fig. 5C). However, the remaining iNKT cells expressed wild-type levels of mature T
308 lymphocyte markers such as CD3 and TCRV β (Fig. 5D).

309

310 ***Parp2*^{-/-} mice have more Ter119⁺-cells than WT mice.**

311 Finally, we eliminated doublets and dead cells, analyzed BM immune cells by flow
312 cytometry to analyze the different immune cell subsets, as depicted in Figure 3A,
313 then we investigated the immune cell subsets in the bone marrow (BM) of *Parp2*^{-/-}
314 mice. As observed in the spleen and the liver, BM cellularity was similar between
315 *Parp2*^{-/-} and WT adult mice (Fig. 6B). The absolute numbers of the different mature
316 BM cell subsets (CD19⁺, GR1^{high} CD11b⁺, GR1^{high} CD11b⁺ and CD3⁺) were
317 similar with slight variations between the two genotypes, except for Ter119 positive
318 cells which were significantly more numerous in *Parp2*^{-/-} mice (Fig. 6C). Similarly, the
319 number of Lin⁻ cells (Ter119⁻ CD19⁻ CD3⁻ GR1⁻ CD11b⁻) was slightly, but not
320 significantly higher in the *Parp2*^{-/-} mice, and was associated with a small increase in
321 the number of the myeloid progenitor (MP) (Lin⁻ ckit⁺ Sca⁻) and LSK populations
322 (Lin⁻ ckit⁺ Sca⁺) (Fig. 6D).

323

324 **DISCUSSION**

325 We previously reported that inhibition of PARP protein activity with the PJ-34 inhibitor
326 protected mice from ConA-induced hepatolysis (2, 14). PARP proteins mediate the
327 activation of various transcription factors, such as NF- κ B, to promote inflammation in
328 several inflammatory diseases, including CCl₄ induced chronic liver injury.
329 Inactivation or inhibition of PARP proteins prevents inflammation-induced tissue
330 damage (4). Inflammation induced by ConA plays a key role in the induction of
331 hepatolysis (12, 13, 17, 21, 25). However, we previously demonstrated that PJ-34
332 does not inhibit inflammation during ConA-induced hepatitis, as cytokine release and
333 liver leucocyte recruitment occurred efficiently, suggesting a more direct role for
334 PARP proteins in the induction of hepatocyte death (2, 14). Here, we show that the
335 genetic inactivation of *Parp2*, but not *Parp1*, protects mice from ConA-induced
336 hepatitis without deregulating inflammation, as leucocyte recruitment and pro-
337 inflammatory cytokine expression were not affected. Analysis of liver and spleen
338 immune populations revealed a substantial reduction in the percentage of iNKT cells,
339 normally enriched in both organs (19). The reduction in the number of iNKT in *Parp2*^{-/-}
340 mice may explain the reduced hepatolysis and protection from ConA-induced
341 hepatitis observed in these mice. Indeed, rapid elimination of NKT cells after ConA
342 treatment is a marker of NKT-induced liver injury following their activation (26). We
343 also observed the elimination of NKT cells after ConA treatment in both *Parp2*^{-/-} and
344 WT mice, but as fewer NKT cells were present in the untreated *Parp2*^{-/-} mice relative
345 to WT mice, there were fewer NKT cells available to induce hepatocyte cell death
346 after ConA treatment in these mice. Surprisingly, whereas IFN- γ is highly produced
347 by NKT cells, we did not observed a reduction of both its expression and its serum
348 level in *Parp2*^{-/-} mice. However in the liver, the reduction of NKT-cell number was

349 compensated by an increase in the number of NK cells which are potent producers of
350 IFN- γ . As a consequence, in *Parp2*^{-/-} mouse liver, the increase of NK cells could
351 compensated the NKT-cell reduction in the inflammatory process. However, the
352 increase in NK-cell number was not sufficient to restore hepatocyte cell death, as
353 ConA-induced liver injury is strictly NKT-dependent and NK-independent (26, 28).
354 Our study using *Parp1* and *Parp2* knockout mice did not allow us to clarify the effect
355 of the PJ-34 inhibitor. Moreover, the fact that *Parp1*^{-/-} mice were not protected against
356 ConA-induced hepatitis, suggests that PARP2 participates in ConA-mediated liver
357 injury, as the two proteins share common functions (1, 8). *Parp1* and *Parp2* double
358 knockout mice are lethal (20). It may be informative to use conditional knockout mice
359 to further decipher the role of both proteins in the liver.

360 We analyzed the thymus and bone marrow of *Parp2*^{-/-} mice to identify the cause of
361 the systemic reduction of iNKT cells detected in these mice. As previously described,
362 *Parp2*^{-/-} mice displayed an increase of the erythroid subset (10), but no T-lymphocyte
363 deregulation. iNKT cells mature in the thymus and are derived from the DP
364 population (11). In agreement with others, we observed a reduction in the number of
365 DP-thymocytes in the absence of PARP2 protein (32) and revealed a substantial
366 reduction in the number of thymic iNKT cells. PARP2 deficiency leads to inefficient
367 V α to J α rearrangement inducing the death of DP-thymocytes (32), resulting in a
368 decrease in the number of mature SP T-lymphocytes and iNKT cells. However, only
369 iNKT-cell numbers were lower in the liver and spleens of adult mice, but not those of
370 conventional T-lymphocytes.

371 The rearrangement of TCR occurs at the DP-thymocyte stage and involves DNA-
372 break and DNA-repair mechanisms. PARP2 is sensitized to DNA damage (8) and
373 has been highlighted to play a role in the TCR α rearrangement process during

374 thymocyte development, as *Parp2*^{-/-} DP thymocytes display a skewed TCRα
375 repertoire and a decrease of cell survival (32). The rearrangement of the TCRα locus
376 occurs in a sequential manner from proximal to distal regions (16) and *Parp2*^{-/-} DP-
377 thymocytes present a reduction of the distal segments Jα42 to Jα4 (32). Interestingly,
378 iNKT cell lineage differentiates at the DP stage and is characterized by expression of
379 an unique TCRα chain with a Vα14-Jα18 rearrangement. As the Jα18 segment is
380 located between the segments Jα42 and Jα4, this strongly suggests that use of Jα18
381 is reduced in DP-thymocyte *Parp2*^{-/-}, and could explain the reduction of iNKT-
382 lymphocyte subset. This is supported by the fact that a default of TCRα
383 rearrangement is known to induce DP-thymocyte cell death (16) and that *Parp2*^{-/-}
384 thymocytes present a shorter lifespan (32).

385

386 In conclusion, previous phenotypic investigations of *Parp2*^{-/-} mice revealed an
387 important role of the PARP2 protein in the regulation of lipid metabolism (24),
388 erythropoiesis (9), thymopoiesis (32) and spermatogenesis (6). Here, we highlight a
389 new phenotype in *Parp2*^{-/-} mice associated with the deregulation of thymopoiesis,
390 resulting in a systemic iNKT deficiency, leading to protection against ConA-induced
391 liver injury.

392

393

394 **Acknowledgements**

395 This work was supported by INSERM, The Ministère de l'Education Nationale de la
396 Recherche et de la Technologie, the University of Rennes 1, the Région Bretagne
397 and the "Ligue Contre le Cancer, Comités du Grand Ouest". AF was supported by a
398 PhD fellowship from the Région Bretagne. We would like to thank the dedicated

399 platforms for immunohistochemistry analysis and animal house facilities (i.e. H2P2
400 and animal house platforms) of SFR BIOSIT, University of Rennes 1, France.

401

402 **References**

- 403 1. **Ame JC, Spenlehauer C, and de Murcia G.** The PARP superfamily. *Bioessays* 26: 882-893,
404 2004.
- 405 2. **Arshad MI, Piquet-Pellorce C, Filliol A, L'Helgoualc'h A, Lucas-Clerc C, Jouan-Lanhouet S,**
406 **Dimanche-Boitrel MT, and Samson M.** The chemical inhibitors of cellular death, PJ34 and
407 Necrostatin-1, down-regulate IL-33 expression in liver. *J Mol Med (Berl)* 93: 867-878, 2015.
- 408 3. **Arshad MI, Piquet-Pellorce C, L'Helgoualc'h A, Rauch M, Patrat-Delon S, Ezan F, Lucas-Clerc**
409 **C, Nabti S, Lehuen A, Cubero FJ, Girard JP, Trautwein C, and Samson M.** TRAIL but not FasL and
410 TNFalpha, regulates IL-33 expression in murine hepatocytes during acute hepatitis. *Hepatology* 56:
411 2353-2362, 2012.
- 412 4. **Bai P and Virag L.** Role of poly(ADP-ribose) polymerases in the regulation of inflammatory
413 processes. *FEBS Lett* 586: 3771-3777, 2012.
- 414 5. **Brenner C, Galluzzi L, Kepp O, and Kroemer G.** Decoding cell death signals in liver
415 inflammation. *J Hepatol* 59: 583-594, 2013.
- 416 6. **Dantzer F, Mark M, Quenet D, Scherthan H, Huber A, Liebe B, Monaco L, Chicheportiche A,**
417 **Sassone-Corsi P, de Murcia G, and Menissier-de Murcia J.** Poly(ADP-ribose) polymerase-2
418 contributes to the fidelity of male meiosis I and spermiogenesis. *Proc Natl Acad Sci U S A* 103: 14854-
419 14859, 2006.
- 420 7. **de Murcia JM, Niedergang C, Trucco C, Ricoul M, Dutrillaux B, Mark M, Oliver FJ, Masson M,**
421 **Dierich A, LeMeur M, Walztinger C, Chambon P, and de Murcia G.** Requirement of poly(ADP-ribose)
422 polymerase in recovery from DNA damage in mice and in cells. *Proc Natl Acad Sci U S A* 94: 7303-
423 7307, 1997.
- 424 8. **De Vos M, Schreiber V, and Dantzer F.** The diverse roles and clinical relevance of PARPs in
425 DNA damage repair: current state of the art. *Biochem Pharmacol* 84: 137-146, 2012.
- 426 9. **Farres J, Llacuna L, Martin-Caballero J, Martinez C, Lozano JJ, Ampurdanes C, Lopez-**
427 **Contreras AJ, Florensa L, Navarro J, Ottina E, Dantzer F, Schreiber V, Villunger A, Fernandez-**
428 **Capetillo O, and Yelamos J.** PARP-2 sustains erythropoiesis in mice by limiting replicative stress in
429 erythroid progenitors. *Cell Death Differ* 22: 1144-1157, 2015.
- 430 10. **Farres J, Martin-Caballero J, Martinez C, Lozano JJ, Llacuna L, Ampurdanes C, Ruiz-Herguido**
431 **C, Dantzer F, Schreiber V, Villunger A, Bigas A, and Yelamos J.** Parp-2 is required to maintain
432 hematopoiesis following sublethal gamma-irradiation in mice. *Blood* 122: 44-54, 2013.
- 433 11. **Gapin L, Matsuda JL, Surh CD, and Kronenberg M.** NKT cells derive from double-positive
434 thymocytes that are positively selected by CD1d. *Nat Immunol* 2: 971-978, 2001.
- 435 12. **Hong F, Jaruga B, Kim WH, Radaeva S, El-Assal ON, Tian Z, Nguyen VA, and Gao B.** Opposing
436 roles of STAT1 and STAT3 in T cell-mediated hepatitis: regulation by SOCS. *J Clin Invest* 110: 1503-
437 1513, 2002.
- 438 13. **Jaruga B, Hong F, Sun R, Radaeva S, and Gao B.** Crucial role of IL-4/STAT6 in T cell-mediated
439 hepatitis: up-regulating eotaxins and IL-5 and recruiting leukocytes. *J Immunol* 171: 3233-3244, 2003.
- 440 14. **Jouan-Lanhouet S, Arshad MI, Piquet-Pellorce C, Martin-Chouly C, Le Moigne-Muller G, Van**
441 **Herreweghe F, Takahashi N, Sergent O, Lagadic-Gossmann D, Vandenamee P, Samson M, and**
442 **Dimanche-Boitrel MT.** TRAIL induces necroptosis involving RIPK1/RIPK3-dependent PARP-1
443 activation. *Cell Death Differ* 19: 2003-2014, 2012.

- 444 15. **Kaneko Y, Harada M, Kawano T, Yamashita M, Shibata Y, Gejyo F, Nakayama T, and**
445 **Taniguchi M.** Augmentation of Valpha14 NKT cell-mediated cytotoxicity by interleukin 4 in an
446 autocrine mechanism resulting in the development of concanavalin A-induced hepatitis. *J Exp Med*
447 191: 105-114, 2000.
- 448 16. **Krangel MS, Carabana J, Abbarategui I, Schlimgen R, and Hawwari A.** Enforcing order within
449 a complex locus: current perspectives on the control of V(D)J recombination at the murine T-cell
450 receptor alpha/delta locus. *Immunol Rev* 200: 224-232, 2004.
- 451 17. **Kusters S, Tiegs G, Alexopoulou L, Pasparakis M, Douni E, Kunstle G, Bluethmann H, Wendel**
452 **A, Pfizenmaier K, Kollias G, and Grell M.** In vivo evidence for a functional role of both tumor necrosis
453 factor (TNF) receptors and transmembrane TNF in experimental hepatitis. *Eur J Immunol* 27: 2870-
454 2875, 1997.
- 455 18. **Luedde T, Kaplowitz N, and Schwabe RF.** Cell death and cell death responses in liver disease:
456 mechanisms and clinical relevance. *Gastroenterology* 147: 765-783 e764, 2014.
- 457 19. **Matsuda JL, Naidenko OV, Gapin L, Nakayama T, Taniguchi M, Wang CR, Koezuka Y, and**
458 **Kronenberg M.** Tracking the response of natural killer T cells to a glycolipid antigen using CD1d
459 tetramers. *J Exp Med* 192: 741-754, 2000.
- 460 20. **Menissier de Murcia J, Ricoul M, Tartier L, Niedergang C, Huber A, Dantzer F, Schreiber V,**
461 **Ame JC, Dierich A, LeMeur M, Sabatier L, Chambon P, and de Murcia G.** Functional interaction
462 between PARP-1 and PARP-2 in chromosome stability and embryonic development in mouse. *EMBO J*
463 22: 2255-2263, 2003.
- 464 21. **Mizuhara H, O'Neill E, Seki N, Ogawa T, Kusunoki C, Otsuka K, Satoh S, Niwa M, Senoh H,**
465 **and Fujiwara H.** T cell activation-associated hepatic injury: mediation by tumor necrosis factors and
466 protection by interleukin 6. *J Exp Med* 179: 1529-1537, 1994.
- 467 22. **Mukhopadhyay P, Rajesh M, Cao Z, Horvath B, Park O, Wang H, Erdelyi K, Holovac E, Wang**
468 **Y, Liaudet L, Hamdaoui N, Lafdil F, Hasko G, Szabo C, Boulares AH, Gao B, and Pacher P.** Poly (ADP-
469 ribose) polymerase-1 is a key mediator of liver inflammation and fibrosis. *Hepatology* 59: 1998-2009,
470 2014.
- 471 23. **Seino K, Kayagaki N, Takeda K, Fukao K, Okumura K, and Yagita H.** Contribution of Fas ligand
472 to T cell-mediated hepatic injury in mice. *Gastroenterology* 113: 1315-1322, 1997.
- 473 24. **Szanto M, Brunyanszki A, Marton J, Vamosi G, Nagy L, Fodor T, Kiss B, Virag L, Gergely P,**
474 **and Bai P.** Deletion of PARP-2 induces hepatic cholesterol accumulation and decrease in HDL levels.
475 *Biochim Biophys Acta* 1842: 594-602, 2014.
- 476 25. **Tagawa Y, Sekikawa K, and Iwakura Y.** Suppression of concanavalin A-induced hepatitis in
477 IFN-gamma(-/-) mice, but not in TNF-alpha(-/-) mice: role for IFN-gamma in activating apoptosis of
478 hepatocytes. *J Immunol* 159: 1418-1428, 1997.
- 479 26. **Takeda K, Hayakawa Y, Van Kaer L, Matsuda H, Yagita H, and Okumura K.** Critical
480 contribution of liver natural killer T cells to a murine model of hepatitis. *Proc Natl Acad Sci U S A* 97:
481 5498-5503, 2000.
- 482 27. **Tiegs G, Hentschel J, and Wendel A.** A T cell-dependent experimental liver injury in mice
483 inducible by concanavalin A. *J Clin Invest* 90: 196-203, 1992.
- 484 28. **Toyabe S, Seki S, Iiai T, Takeda K, Shirai K, Watanabe H, Hiraide H, Uchiyama M, and Abo T.**
485 Requirement of IL-4 and liver NK1+ T cells for concanavalin A-induced hepatic injury in mice. *J*
486 *Immunol* 159: 1537-1542, 1997.
- 487 29. **Trautwein C, Rakemann T, Brenner DA, Streetz K, Licato L, Manns MP, and Tiegs G.**
488 Concanavalin A-induced liver cell damage: activation of intracellular pathways triggered by tumor
489 necrosis factor in mice. *Gastroenterology* 114: 1035-1045, 1998.
- 490 30. **Virag L, Robaszekiewicz A, Rodriguez-Vargas JM, and Oliver FJ.** Poly(ADP-ribose) signaling in
491 cell death. *Mol Aspects Med* 34: 1153-1167, 2013.
- 492 31. **Watanabe Y, Morita M, and Akaike T.** Concanavalin A induces perforin-mediated but not
493 Fas-mediated hepatic injury. *Hepatology* 24: 702-710, 1996.

- 494 32. **Yelamos J, Monreal Y, Saenz L, Aguado E, Schreiber V, Mota R, Fuente T, Minguela A,**
495 **Parrilla P, de Murcia G, Almarza E, Aparicio P, and Menissier-de Murcia J.** PARP-2 deficiency affects
496 the survival of CD4+CD8+ double-positive thymocytes. *EMBO J* 25: 4350-4360, 2006.
497 33. **Zheng SJ, Wang P, Tsabary G, and Chen YH.** Critical roles of TRAIL in hepatic cell death and
498 hepatic inflammation. *J Clin Invest* 113: 58-64, 2004.

499

500

501 **Figures legends**

502 **Figure 1: The absence of PARP2 but not PARP1 protects mice from ConA**
503 **induced-hepatitis.** (A) Serum levels of serum AST and ALT in WT, *Parp1*^{-/-}, and
504 *Parp2*^{-/-} mice, 11 h after PBS (n = 4 to 6) or ConA injection (n =1 3 for WT, 8 for
505 *Parp1*^{-/-}, and 24 for *Parp2*^{-/-}). (B) Representative images of H&E stained liver tissue
506 sections, necrosis areas are outlined by the white dotted line. (C) Serum levels of
507 ALT of WT or *Parp2*^{-/-} mice 24 h after ConA treatment. (D) Levels of liver TNF- α , IFN- γ ,
508 IL-1 β , and IL-4 transcripts from WT, *Parp1*^{-/-}, and *Parp2*^{-/-} mice 11 h after ConA
509 administration. (E) Serum levels of TNF- α , IFN- γ and IL-6 in WT and *Parp2*^{-/-} mice, 11
510 h after PBS (n = 4 to 6) or ConA injection (n= 6 to 11). For the scatter plots, errors
511 bars represent + SEM. (* #p < 0.05; ** ## p < 0.01; *** ### p < 0.001; ns: non-
512 significant).

513

514 **Figure 2: PARP2 deficiency results in a decrease in the number of liver iNKT**
515 **cells.** (A) Gating strategy used to analyze lymphocyte subpopulations (NKT, NK, T
516 cells, B cells) and myeloid cells in the liver and spleen. The gating strategy for liver
517 immune cells is presented. (B) Absolute number of liver immune cells. (C) Absolute
518 number of T lymphocytes (CD3+ TCRVb+*NK1.1*-), CD4-positive cells (in black) and
519 CD8-positive cells (in white). (D) Absolute number of NKT cells (CD3+
520 TCRVb+*NK1.1*-) in the liver (E) Representative dot plot showing NKT subsets in the
521 liver (left panel) and absolute number of liver iNKT cells (corresponding to
522 aGalCer+CD4+ and aGalCer+CD4- cells) (middle panel) and liver NKT DN-cells
523 (aGalCer-CD4-) (right panel). (F) Representative dot plot showing liver NK-cell
524 population (left part) and absolute number of liver NK cells (*NK1.1*+CD3-) (right
525 panel). (G) Absolute number of liver B-lymphocytes (CD19+CD11b) and (H) myeloid

526 cells (GR1^{int}CD11b+ and GR1^{high}CD11b+). All suspensions of liver immune cells from
527 non-treated mice, aged 5 or 10 to 12 weeks, were obtained from the livers of WT or
528 *Parp2*^{-/-} mice. Each dot in the graph represents the number of cells recovered from
529 one liver. The line and error bars represent the mean +/- SEM. For the histograms,
530 the errors bars represent + SD. (* #p < 0.05; ** ## p < 0.01; *** ### p < 0.001; ns:
531 non-significant).

532

533 **Figure 3: PARP2 deficiency does not affect ConA-induced liver-leucocyte**
534 **recruitment or activation.** (A) Absolute number of liver immune cells from WT or
535 *Parp2*^{-/-} adult mice, non-treated (Ctl) or treated with ConA. Immune cells were
536 isolated 11 or 24 h after ConA treatment. (B) Absolute number of NKT-cells from the
537 livers of WT or *Parp2*^{-/-} mice at steady state (Ctl) or 11 h after ConA treatment. (C)
538 Absolute number of lymphocytes: T cells, B cells, and NK cells (upper panel) and
539 myeloid cells (lower part) from liver of WT or *Parp2*^{-/-} mice at steady state or 11 h
540 after ConA treatment. (D) Representation of the activation marker (CD69) of T-
541 lymphocytes CD8+ (NK1.1-TCRVb+CD3+CD8+) in the liver of WT or *Parp2*^{-/-} mice
542 treated or not with ConA. The line and error bars represent the mean + SD (* #p <
543 0.05; ** ## p < 0.01; *** ### p < 0.001; ns: non-significant).

544

545 **Figure 4: PARP2 deficiency results in a reduction in the number of iNKT cells in**
546 **the spleen.** (A) Number of splenocytes of non-treated WT and *Parp2*^{-/-} mice, aged 5
547 (early adult mice) or 10 at 12 weeks (adult mice). (B) Percentage of T lymphocytes
548 (CD3+), TCRVb+NK1.1-), (C) B-ymphocytes (CD19+CD11b-), (D) total NKT cells
549 (CD3+TCRVb+NK1.1+) (left panel), and NKT subsets: iNKT (NKT, α-GalCer+) (middle
550 panel) and NKT-DN (NKT, α-GalCer- CD4-) (right panel), (E) NK cells (CD3-NK1.1+)

551 determined by flow cytometry analysis from spleens of early-adult or adult WT and
552 *Parp2*^{-/-} mice. Each dot in the graph represents the number of cells recovered from
553 one liver. The lines and error bars represent the mean +/- SEM. (* p <0.05; ** p <
554 0.01; *** p < 0.001; ns: non-significant).

555

556 **Figure 5: PARP2 deficiency results in a decreased number of CD4/CD8 DP and**
557 **SP cells as well as iNKT cells.** (A) Representative staining profiles of CD4 and CD8
558 single or double positive cells from the thymus of non-treated five-week-old WT or
559 *Parp2*^{-/-} mice. (B) Graph showing total number and the number of CD4⁺CD8⁺ double
560 positive thymocytes. (C) Representative staining profile of α GalCer positive
561 thymocytes. (D) Representation of mature T-cell markers (CD3 and TCRV β) of
562 α GalCer positive thymocytes. Each dot in the graph represent the number of cells
563 recovered from one liver. The lines and errors bars represent the mean +/- SEM. (*
564 p<0.05; ** p<0.01; *** p<0.001; ns: non-significant).

565

566 **Figure 6: *Parp2*^{-/-} mice display an increased number of Ter119⁺-cells but not of**
567 **other mature or immature subsets.** (A) Gating strategy used to analyze bone
568 marrow immune cell subsets. (B) Absolute number of cells recovered from two
569 femurs of WT or *Parp2*^{-/-} adult (10 at 12 weeks old) mice. (C) Absolute cell number
570 for each mature bone marrow immune cells subset: Ter119⁺, CD19⁺, CD3⁺,
571 GR1^{high}CD11b⁺, and GR1^{int}CD11b⁺. (D) Absolute number of immature Lin⁻ bone
572 marrow immune cells (Ter119⁻ CD19⁻ CD3⁻ GR1⁻ CD11b⁻) (left panel) and the specific
573 MP (Lin⁻ckit⁺Sca⁻) and LSK (Lin⁻ckit⁺Sca⁺) subsets (right panel). Each dot in the
574 graph represents the number of cells recovered from one liver. The lines and errors

575 bars represent the mean \pm SEM. (* $p < 0.05$; ** $p < 0.01$; *** $p < 0.001$; ns: non-
576 significant).

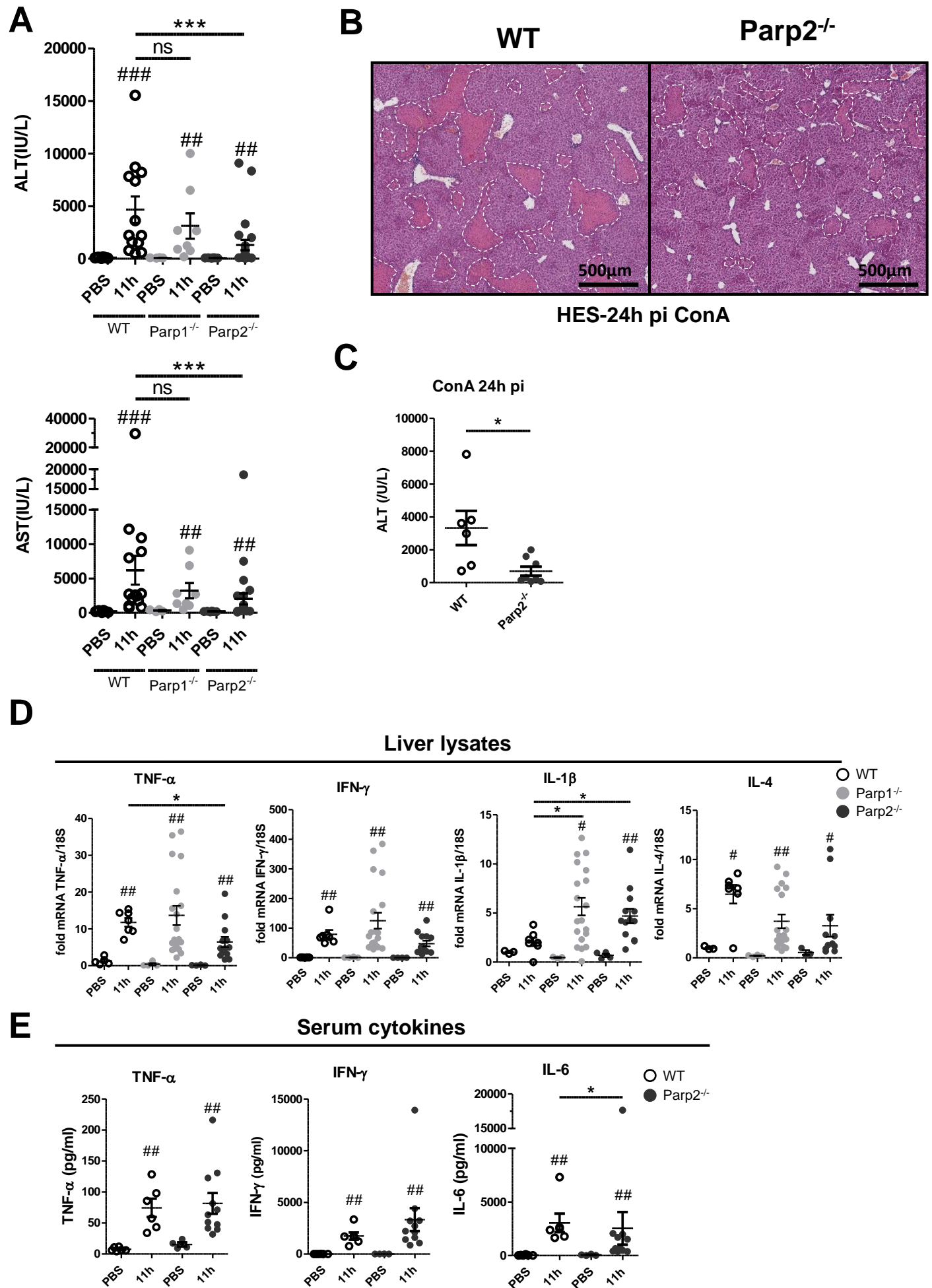
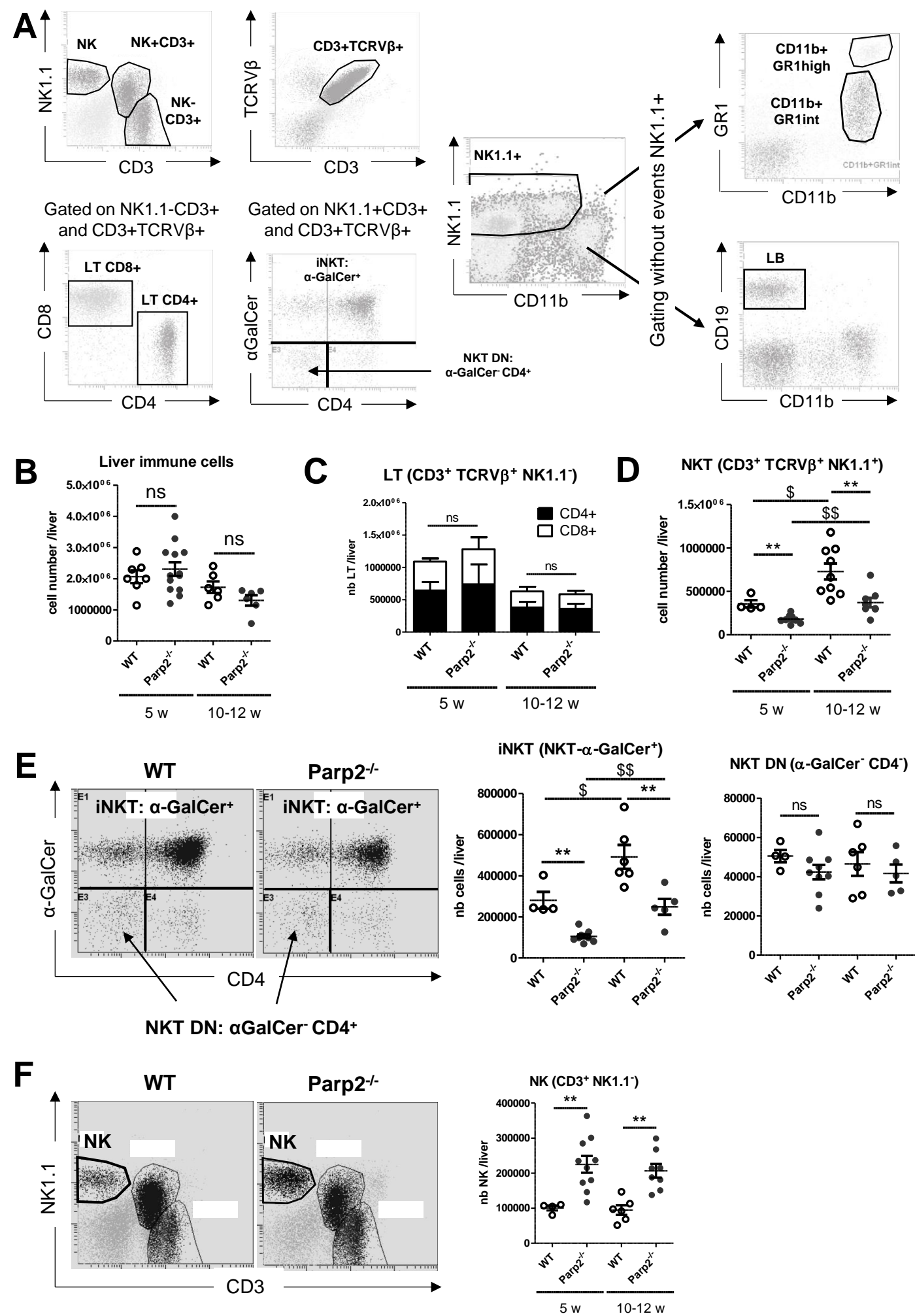
Figure 1

Figure 2

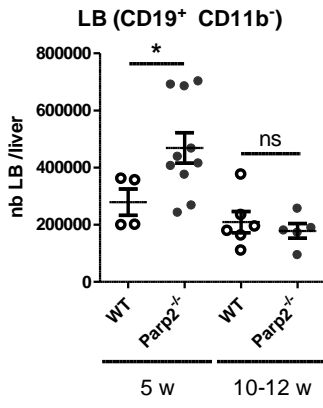
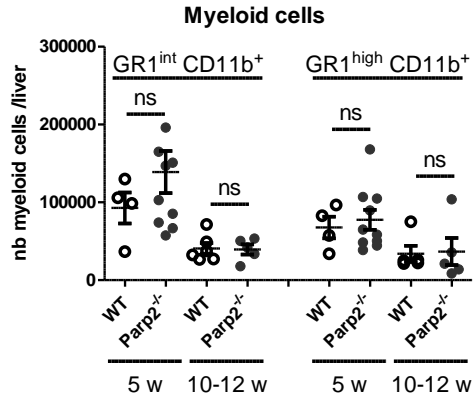
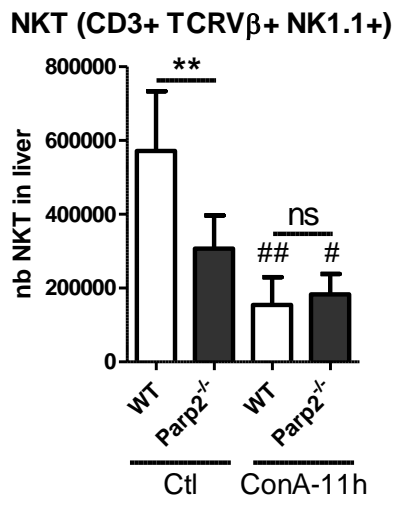
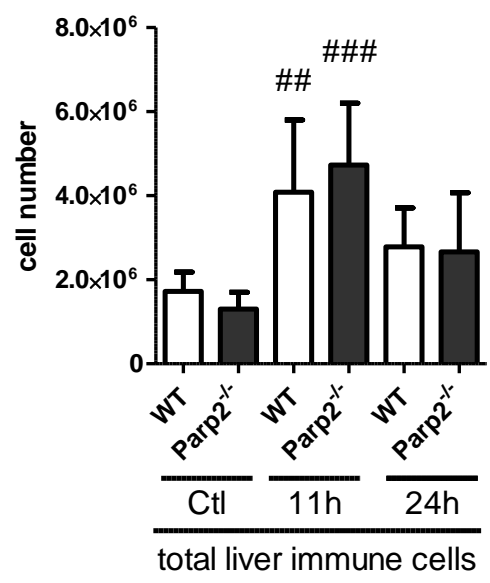
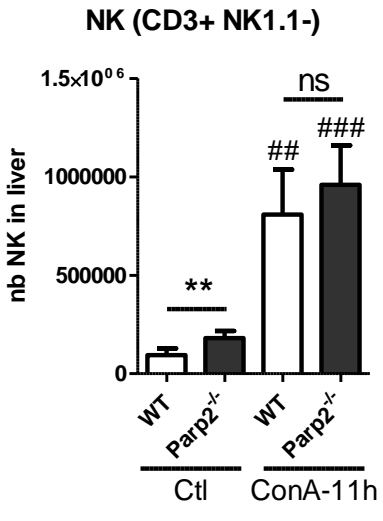
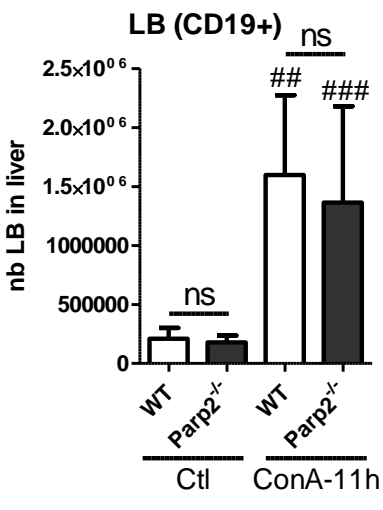
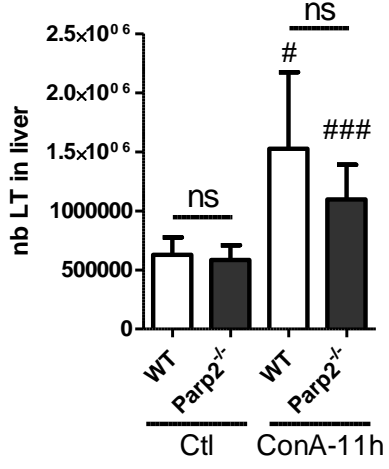
G**H**

Figure 3

A ConA (12 mg/kg) B



C LT (CD3+ TCRVβ+ NK1.1-) LB (CD19+) NK (CD3+ NK1.1-)



GR1^{int} CD11b+ GR1^{high} CD11b+

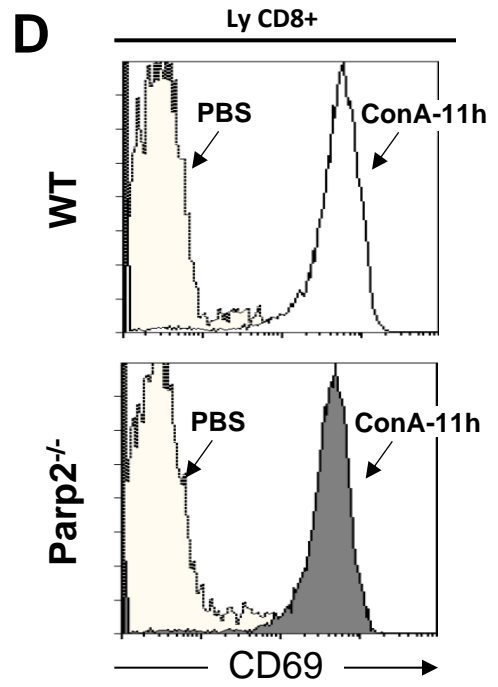
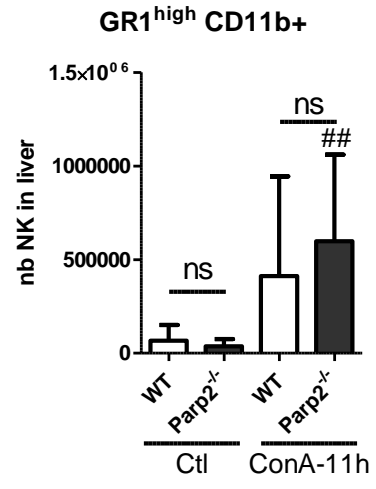
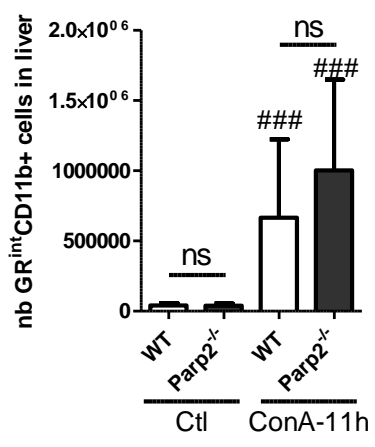


Figure 4

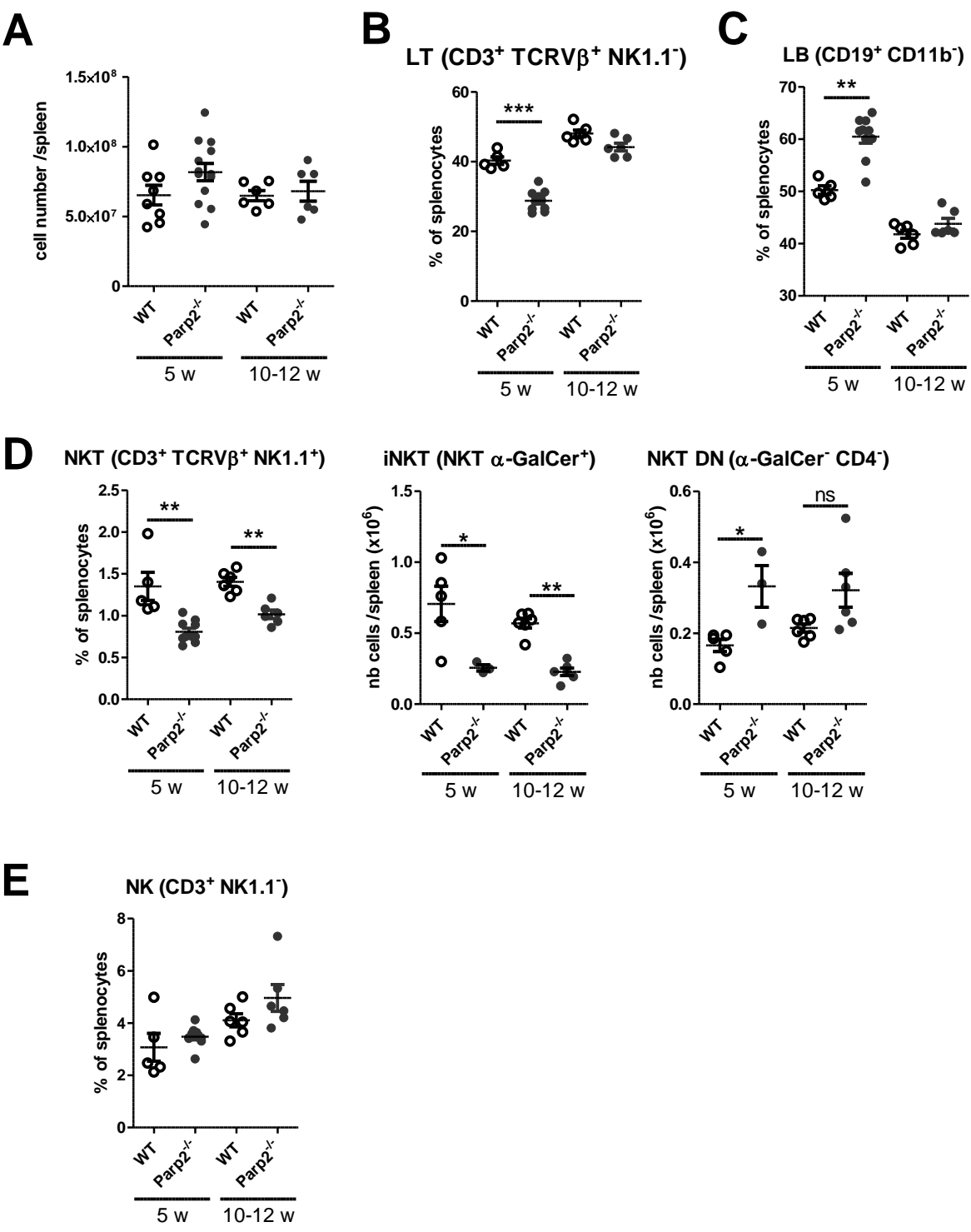


Figure 5

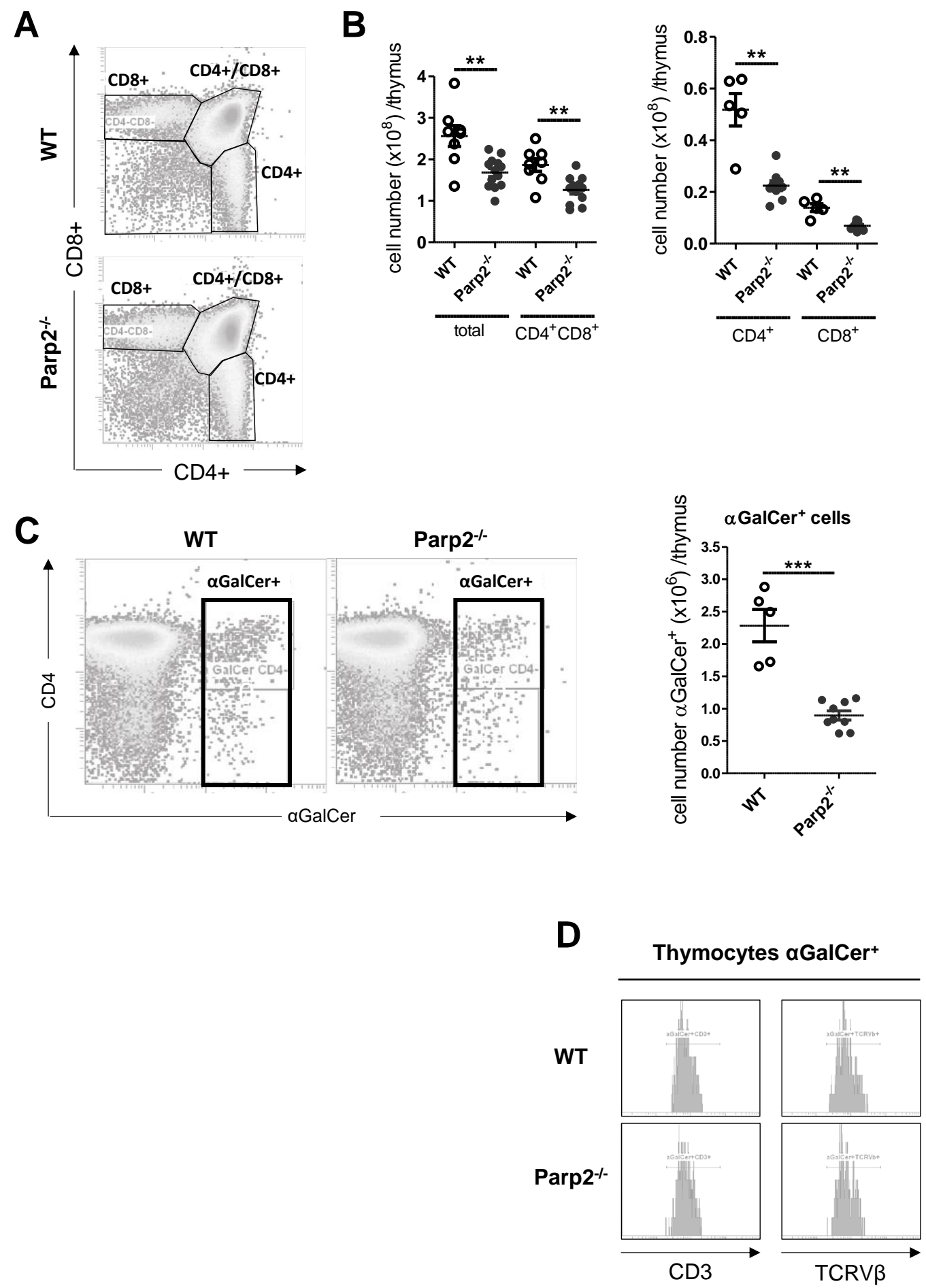
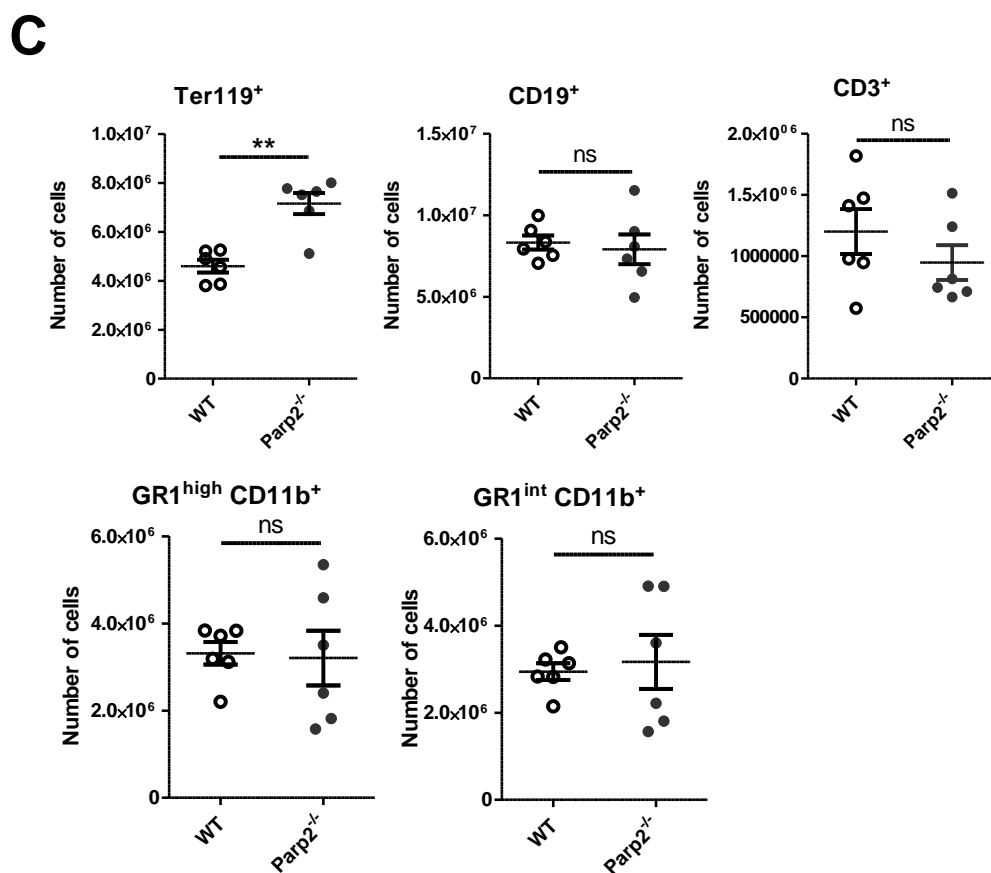
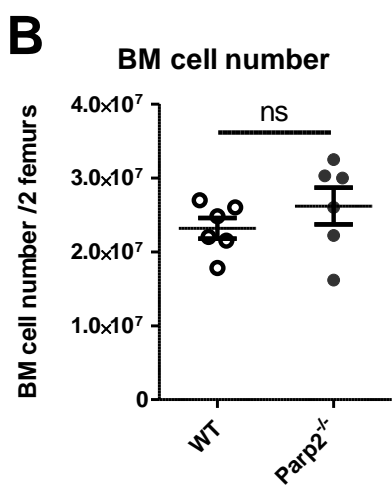
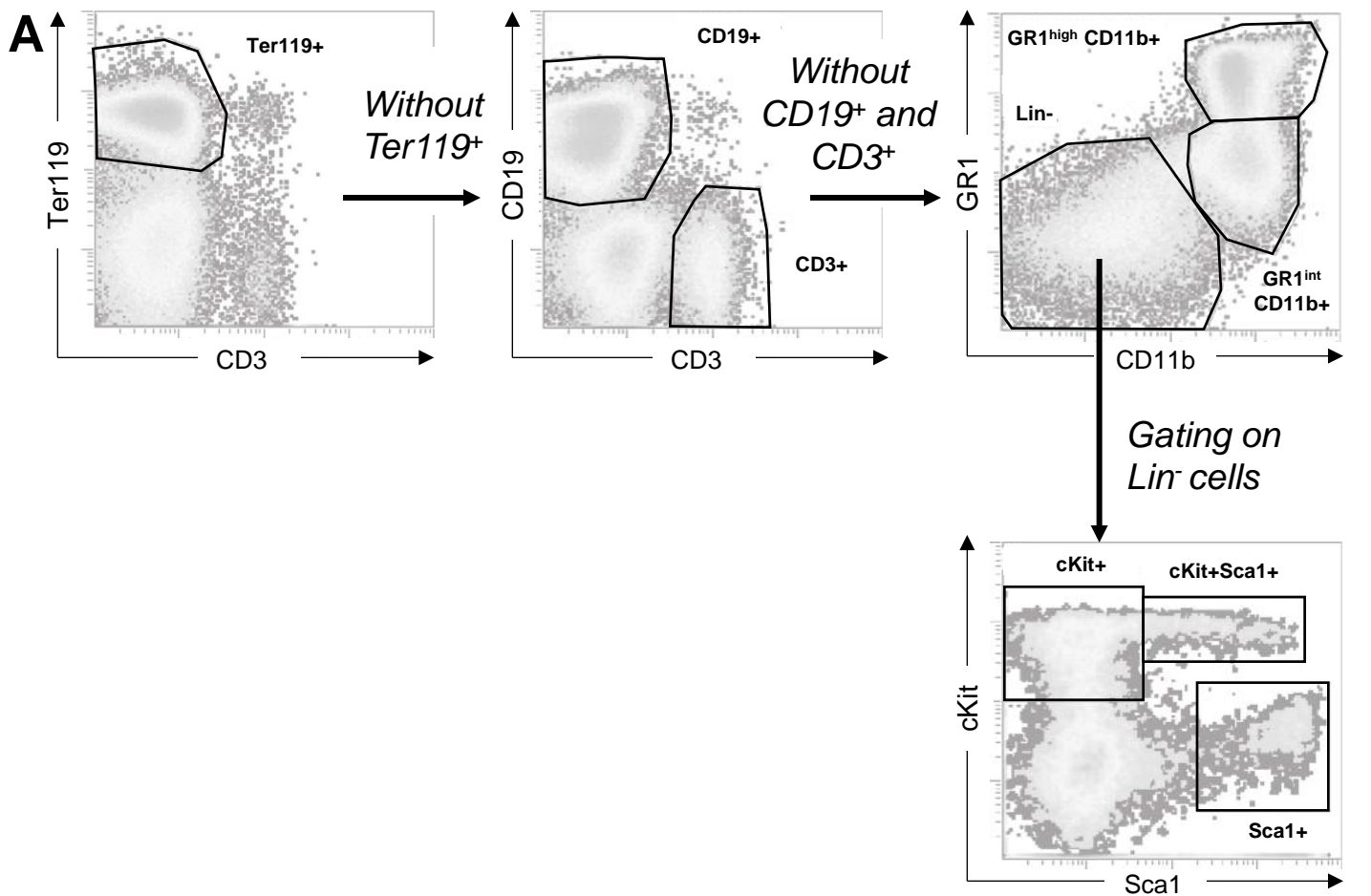


Figure 6

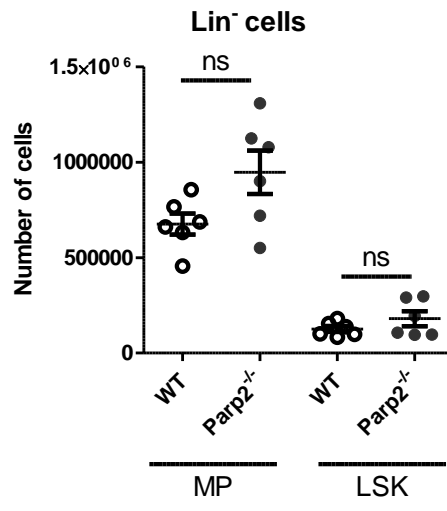
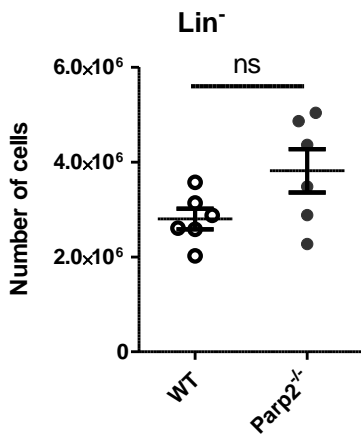
D

Table 1. Sequence of primers used for qPCR

Gene	Forward	Reverse
Mouse 18S	5'-CGCCGCTAGAGGTGAAATTC-3'	5'-TTGGCAAATGCTTTCGCTC-3'
Mouse TNF α	5'-TAGCTCCCAGAAAAGCAAGC-3'	5'-TTTTCTGGAGGGAGATGTGG-3'
Mouse IFN- γ	5'AGGTCAACAACCCACAGGTC3'	5'ATCAGCAGCGACTCCTTTTC3'
Mouse IL-1 β	5'-GAAGAAGTGCCCATCCTCTG-3'	5'-AGCTCATATGGGTCCGACAG-3'
Mouse IL-4	5'-GGCTTCCAAGGTGCTTGG-3'	5'-GGACTTGGACTCATTGATGG-3'